Development of the LBNL Positron Emission Mammography Camera

J. S. Huber, *Member, IEEE*, W. S. Choong, *Member, IEEE*, J. Wang, *Member, IEEE*, J. S. Maltz, *Member, IEEE*, J. Qi, *Member, IEEE*, E. Mandelli, *Member, IEEE*, and W. W. Moses, *Senior Member, IEEE*

***Abstract*—We present the construction status of the LBNL positron emission mammography (PEM) camera, which utilizes a positron emission tomography (PET) detector module with depth of interaction measurement consisting of 64 LSO crystals ($3 \times 3 \times 30\ \mathrm{mm}^3$) coupled on one end to a single photomultiplier tube (PMT) and on the opposite end to a 64 pixel array of silicon photodiodes (PDs). The PMT provides an accurate timing pulse, the PDs identify the crystal of interaction, the sum provides a total energy signal, and the $\mathrm{PD}/(\mathrm{PD}+\mathrm{PMT})$ ratio determines the depth of interaction. We have completed construction of all 42 PEM detector modules. All data acquisition electronics have been completed, fully tested and loaded onto the gantry. We have demonstrated that all functions of the custom IC work using the production rigid-flex boards and data acquisition system. Preliminary detector module characterization and coincidence data have been taken using the production system, including initial images.**

***Index Terms*—Biomedical imaging, detectors, positron emission tomography (PET).**

I. Introduction

THIS paper describes the status and construction of the LBNL positron emission mammography (PEM) camera [1]. The breast is inserted in the gap between the top and bottom $7.5 \times 10\ \mathrm{cm}^2$ detector planes, and the spacing between planes adjusted to provide light compression on the breast. The positions of the $7.5 \times 7.5\ \mathrm{cm}^2$ detector planes on the left and right of the breast are fixed. The active portion of the detector (i.e., the portion sensitive to 511 keV photons) is divided into $2.5 \times 2.5 \times 3.0\ \mathrm{cm}^3$ detector modules. Each detector module is further divided into 64 individual LSO scintillation crystals, each $3 \times 3 \times 30\ \mathrm{mm}^3$. We have currently instrumented only the two side ($7.5 \times 7.5\ \mathrm{cm}^2$) detector planes, using 18 detector modules.

We have previously reported on a PET detector module capable of measuring depth of interaction on an event by event basis [2], [3], shown in Fig. 1. With this design, a single photomultiplier tube (PMT) provides an accurate timing pulse and initial energy discrimination for an 8×8 array of LSO [4] scintillator crystals, an 8×8 silicon photodiode array (PDs) identifies the crystal of interaction, the $\mathrm{PD}/(\mathrm{PD}+\mathrm{PMT})$ ratio measures the depth of interaction, and the sum (PD + PMT) provides a total energy signal. We are planning to use this PET detector module in several tomograph designs [1], [5], [6]; thus, we have transformed our prototype detector into one that can be produced in quantity.

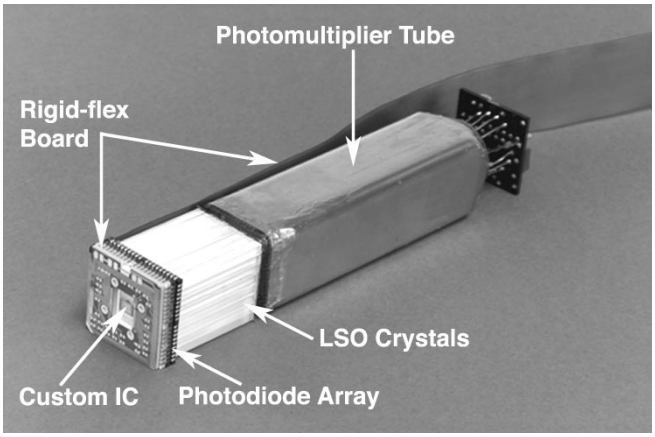

Fig. 1. Photograph of the PET detector. Each crystal is attached to a photomultiplier tube and photodiode. The PMT and PD signals are combined to measure the depth of interaction and total energy. The custom integrated circuit is mounted on a rigid-flex board with a Kapton tail that goes between adjacent detector modules to act as a cable connecting the IC to the remainder of the readout electronics.

We focus in this paper on new results using production versions of the complete system—custom ICs, rigid-flex boards (used to read out the IC), detector modules, and data acquisition system. The major milestone of reading out coincidence data with the production system has been achieved, and initial images are shown.

II. System

A. Detector Modules

We have built all 42 production detector modules to be used in our PEM camera design [1]. Fig. 1 shows a photograph of one production detector module. The end-on "profile" of the module is 2.5 cm square, allowing close packing of multiple detector modules in two dimensions. Communication between the custom integrated circuit (PETRIC) [7] and the remainder of the electronics [8] (which is located "behind" the photomultiplier tube) is accomplished by a 0.008″ thick Kapton "flex tail" on the IC printed circuit board that is thin enough to run between adjacent detector modules. The successful production of these rigid-flex boards has proved to be a surprisingly difficult task, but we are now taking data using the working, final ver-

Manuscript received December 20, 2002; revised April 28, 2003. This work was supported in part by the Director, Office of Science, Office of Biological and Environmental Research, Medical Science Division, U.S. Department of Energy under Contract DE-AC03-76SF00098, and in part by Public Health Service Grant RO1-CA67911. Reference to a company or product name does not imply approval or recommendation by the University of California or the U.S. Department of Energy to the exclusion of others that may be suitable.

The authors are with the Lawrence Berkeley National Laboratory, Berkeley, CA 94720 USA (e-mail: jshuber@lbl.gov).

Digital Object Identifier 10.1109/TNS.2003.817941

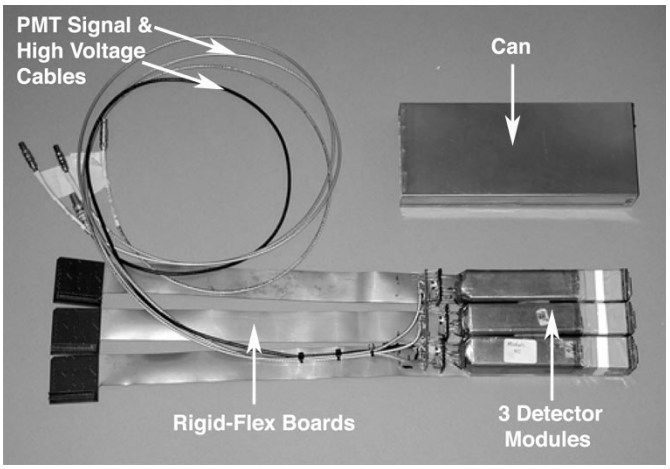

Fig. 2. Photograph of the detector "can" assembly. Rigid-flex boards are attached to each detector module's photodiode. Three detector modules are then attached to a high voltage distribution board and assembled into a light-tight can.

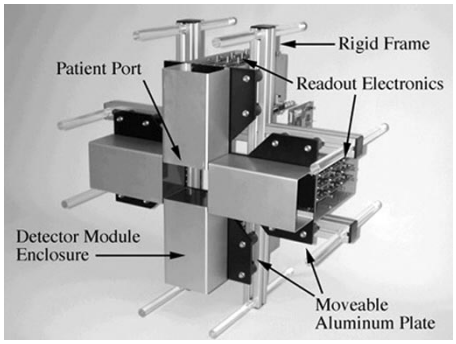

Fig. 3. A photograph of the actual PEM gantry which is fully loaded with the complete data acquisition electronics (but not loaded with detector modules). Each detector bank utilizes nine (side bank) or 12 (top/bottom bank) detector modules. The detector modules are loaded into a can (Fig. 2) with the Kapton "flex tail" feeding out between the detector modules and connecting to the readout electronics.

sions of the rigid-flex boards. All functions of the PETRIC chip (including the winner-take-all circuitry for analog and channel address selection of the "winner") have been demonstrated to work with production rigid-flex boards and the final data acquisition system.

The detector module assembly process is complete. We are now in the process of attaching rigid-flex boards onto each detector module's photodiode, as well as bundling three detector modules (with rigid-flex boards) and assembling them into light-tight cans. Fig. 2 shows the details of our "can" assembly. Currently, half of the detector modules have been assembled into cans.

B. Camera

We have instrumented the two side $(7.5 \times 7.5\,\mathrm{cm}^2)$ detector banks, using 18 detector modules (i.e., 3 detector cans per bank). Fig. 3 shows the camera gantry and electronics before the modules were put in place.

The detector modules are read out with electronics originally developed by CPS Innovations (Knoxville, TN) for the HRRT brain imaging PET camera and modified to use a detector module that incorporates a photodiode [8]. The top level

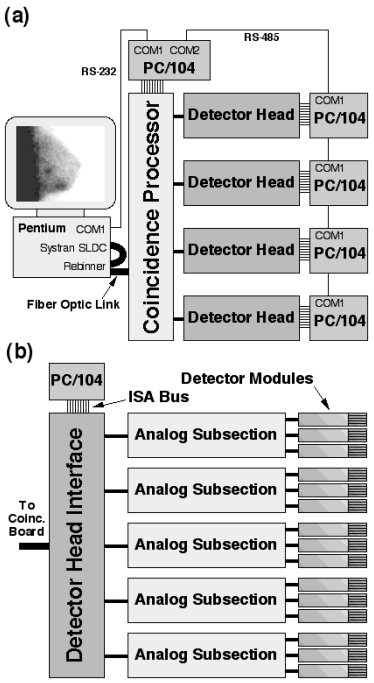

Fig. 4. (a) Top level diagram of the electronics system. Each of the four detector hands collects "singles" events which are forwarded to the coincidence processor. Coincident events are then passed to the computer via a fiber optic link. A rebinner board can optionally be placed between the coincidence processor and the fiber optic readout board. (b) Diagram of a detector head. Three detector modules are serviced by each analog subsection board. The singles event words generated by the Analog Subsection board are multiplexed by the DHI board, which also buffers communication with the PC/104 as well as system timing signals [8].

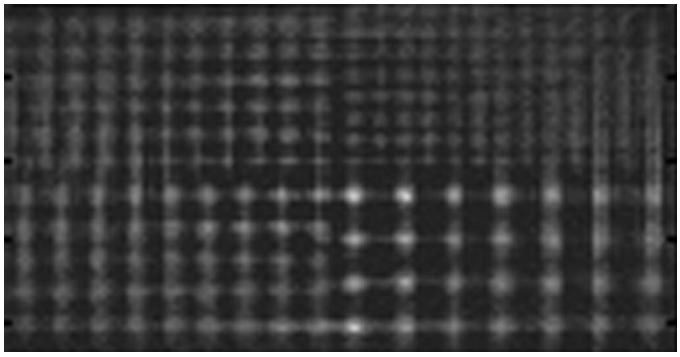

Fig. 5. Simulated spherical sources located at the central plane. The spheres are arranged where the distances between the sources are four times their diameters (like a Derenzo Phantom). The diameters are 1.0, 1.25, 1.5, and 2.0 mm.

diagram of the electronics system is shown in Fig. 4(a), and the diagram of a detector head is shown in Fig. 4(b). The outputs of three detector modules are processed by an analog subsection board. Events are detected and assigned an arrival time, the crystal of interaction is identified, energy qualification is performed, and a digital word is formed. The output signals from the analog subsection boards are then multiplexed by detector head interface (DHI) boards. A CPS coincidence processor identifies singles events from different DHI boards that are in coincidence, and the output is sent to a Pentium-based computer system that accumulates the coincident data, reconstructs the images, and displays them.

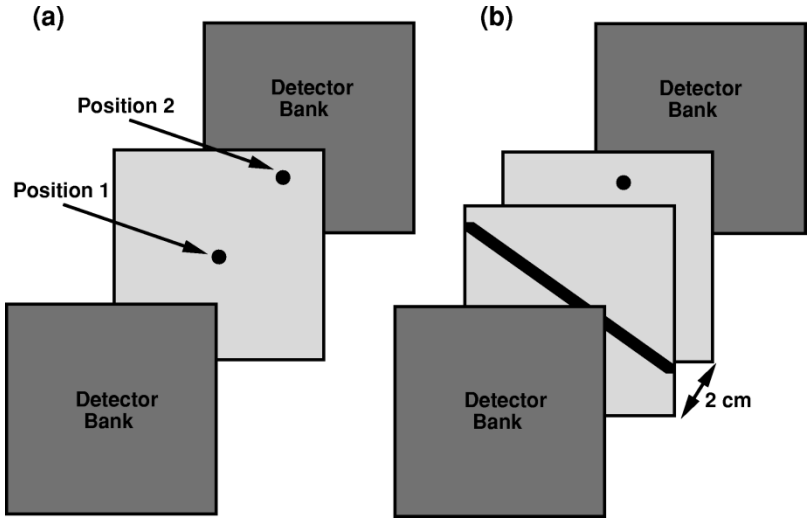

Fig. 6. Geometry for data taking, with $^{68}\mathrm{Ge}$ sources placed between two opposing planar detector banks. The distance between detector banks was 7 cm. (a) In the first setup, a point source in the mid-plane was used. Data was taken at two different point source positions. (b) In the second setup, a point and rod source in different planes were used. The point source (1.5 mm diameter, 106 μCi) was in the mid-plane and the rod source (2.5 mm diameter, 118 μCi) was in a plane that was 2 cm away.

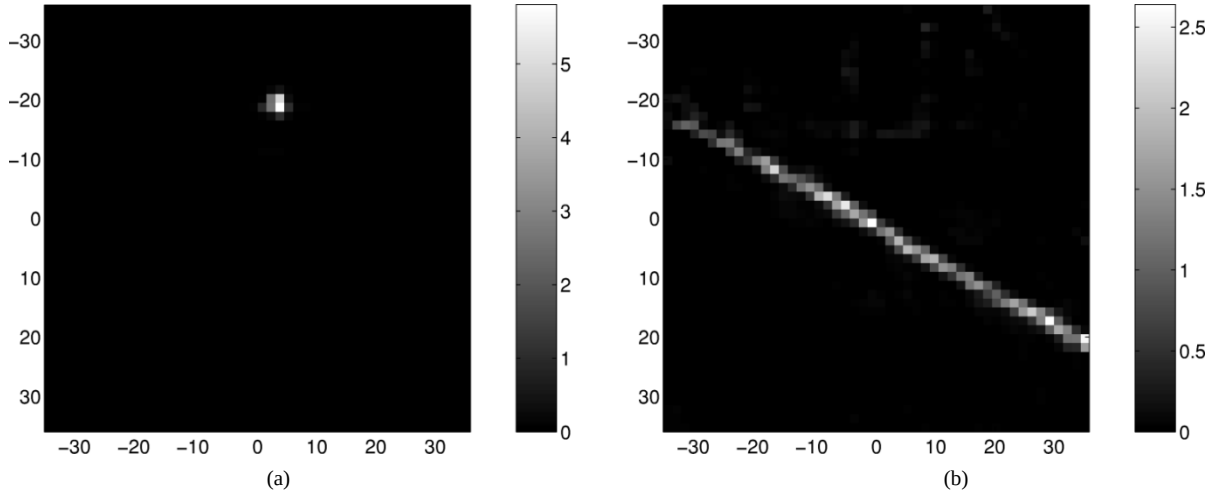

Fig. 7. Images of the (a) 1.5 mm diameter $^{68}\mathrm{Ge}$ point source (106 μCi) placed in the mid-plane and (b) 2.5 mm diameter rod source (118 μCi) placed in a different plane (2 cm away), as described in Fig. 6(b). The x- and y-scale are in millimeters. The vertical intensity scale ranges from $0 - 5 \times 10$au for (a) and from $0 - 2.5 \times$ au for (b). The reconstruction was done using 10 M events. The point source has (3.00, 2.25) mm FWHM reconstruction resolution.

This final data acquisition system was used to calibrate the detector modules. We have automated calibration software that sets up the electronics and identifies bad channels using test pulses. In addition, we have automated software that acquires (singles or coincidence) data with a $^{68}\mathrm{Ge}$ source (using the PMT signal with a low discriminator threshold for triggering), corrects for channel to channel gain variation in the PMT signal, and rejects events with PMT signal outside the 350–700 keV energy window. However, we currently have not corrected for channel to channel gain variation in the PD signal, and have not scaled the relative PD and PMT signal; thus we have not yet been able to calculate the depth of interaction (DOI) with the production system. Since the calibration procedure is not complete [9], the PD is only used to identify the crystal of interaction.

C. Reconstruction

We have developed and tested both filtered backprojection reconstruction algorithms (2-D [10] and 3-D [11]) and a list mode regularized maximum likelihood reconstruction algorithm [12] using simulated data. The rectangular geometry and the capability of measuring DOI result in irregular sampling in the sinogram space. In the filtered backprojection algorithm, data are rebinned onto a regular grid. In the list mode maximum likelihood algorithm, the irregular sampling and DOI information are explicitly modeled in the projection matrix. To demonstrate the expected system performance, Fig. 5 shows a reconstructed image of simulated spherical sources using the 3-D filtered backprojection algorithm. The resolution of the reconstruction varies from 1.54 mm full width at half maximum (FWHM) at the center to 3.10 mm at the corner. As the current camera setup only contains two opposing detector banks, the filtered backprojection algorithm is not directly applicable. Therefore, in Section III we only show the list mode maximum likelihood reconstruction of the real data.

III. Results

The two instrumented detector banks were used to image $^{68}\mathrm{Ge}$ sources in two different configurations, as shown in Fig. 6.

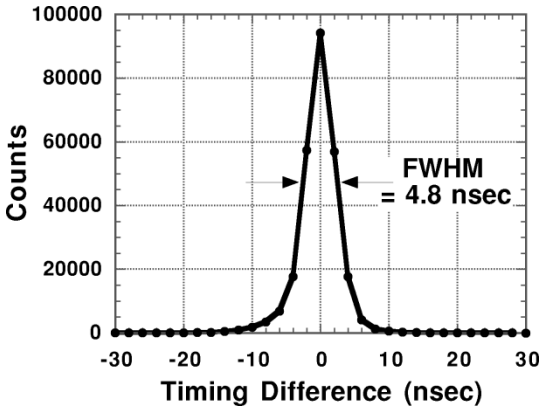

Fig. 8. The spectrum of the timing difference between two detector modules with the 1.5 mm diameter ^{68}Ge point source (106 μCi) placed in the mid-plane. Only the PMT information was used, with a low energy threshold. No channel to channel corrections were made. The preliminary coincidence timing resolution is 4.8 nsec FWHM.

The distance between the opposing detector banks was 7 cm. In the first setup, a 1.5 mm diameter ^{68}Ge point source (106 μCi) was placed in the mid-plane between the two planar detector banks. Data was taken at two different point source positions (Fig. 6(a)), resulting in 10 M events each. The images were reconstructed with the maximum likelihood algorithm using $1.5 \times 1.5 \times 3\ \mathrm{mm}^3$ voxels. Normalization factors were measured using a plane source placed in the mid-plane. The reconstructed point in position 1 has an in-plane (1.65, 2.85) mm FWHM reconstruction resolution. In position 2, the in-plane reconstruction resolution is (2.40, 1.95) mm FWHM. The variation in FWHM is mostly caused by the misalignment between the point source position and the voxel grid. The nonnegativity constraint in the maximum likelihood reconstruction did not have a large impact on the resolution measurement here, as we obtained similar results when we reconstructed the point source data after superimposing it with a simulated uniform background.

In the second setup, a point and rod source in different planes were used. The 1.5 mm diameter ^{68}Ge point source (106 μCi) was placed in the mid-plane and a 2.5 mm diameter rod source (118 μCi) was placed in a plane that was 2 cm apart [Fig. 6(b)]. Fig. 7 shows the images of the rod and point source with 10 M events. The point source has (3.00, 2.25) mm FWHM reconstruction resolution. Since the concentration of activity in the point source is much stronger than the rod source, background activity in the area of the point source is seen in the rod source plane.

Fig. 8 shows the spectra of the timing difference between two production detector modules, which were read out with the final data acquisition system. Data was taken using the 1.5 mm diameter ^{68}Ge point source (106 μCi) placed in the mid-plane between the two detector modules. Only the PMT information was used, with a low energy threshold. While channel to channel corrections are planned, none were used to acquire these data. The preliminary coincidence timing resolution is 4.8 nsec FWHM.

IV. Discussion and Conclusion

Two significant tasks remain before this camera is complete: assembly of the remaining two detector banks needs to be finished and the remainder of the calibration algorithms (especially for the photodiode) needs to be developed. However, we feel that major milestones have been achieved with our system. All components are complete—custom ICs, rigid-flex boards, detector modules, data acquisition electronics and the gantry. Production firmware and calibration has been developed. Most importantly, the first images have been acquired using two opposing banks of 3×3 modules each. Initial reconstruction resolutions are in agreement with expectation.

Acknowledgment

The authors would like to thank G. Zizka for his assistance in wire bonding. They would also like to thank CPS Innovations (Knoxville, TN) for providing electronics and technical assistance.

References

[1] W. W. Moses, T. F. Budinger, and R. H. Huesman *et al.*, "PET camera designs for imaging breast cancer and axillary node involvement," *J. Nucl. Med.*, vol. 36, p. 69P, 1995.

[2] J. S. Huber, W. W. Moses, and S. E. Derenzo *et al.*, "Characterization of a 64 channel PET detector using photodiodes for crystal identification," *IEEE Trans. Nucl. Sci.*, vol. 44, pp. 1197–1201, June 1997.

[3] J. S. Huber, W. W. Moses, and M. S. Andreaco *et al.*, "An LSO scintillator array for a PET detector module with depth of interaction measurement," *IEEE Trans. Nucl. Sci.*, vol. 48, pp. 684–688, June 2001.

[4] C. L. Melcher and J. S. Schweitzer, "Cerium-doped lutetium oxyorthosilicate: a fast, efficient new scintillator," *IEEE Trans. Nucl. Sci.*, vol. 39, pp. 502–505, Aug. 1992.

[5] W. W. Moses, P. R. G. Virador, and S. E. Derenzo *et al.*, "Design of a high-resolution, high-sensitivity PET camera for human brains and small animals," *IEEE Trans. Nucl. Sci.*, vol. 44, pp. 1487–1491, Aug. 1997.

[6] J. S. Huber and W. W. Moses, "Conceptual design of a high sensitivity small animal PET camera with 4π coverage," *IEEE Trans. Nucl. Sci.*, vol. 46, pp. 498–502, June 1999.

[7] M. Pedrali-Noy, G. J. Gruber, and B. Krieger *et al.*, "PETRIC—a positron emission tomography readout IC," *IEEE Trans. Nucl. Sci.*, vol. 48, pp. 479–484, June 2001.

[8] W. W. Moses, J. W. Young, and K. Baker *et al.*, "The electronics system for the LBNL positron emission mammography (PEM) camera," *IEEE Trans. Nucl. Sci.*, vol. 48, pp. 632–636, June 2001.

[9] J. S. Huber, W. W. Moses, and P. R. G. Virador, "Calibration of a PET detector module that measures depth of interaction," *IEEE Trans. Nucl. Sci.*, vol. 45, pp. 1268–1272, June 1998.

[10] P. R. G. Virador, W. W. Moses, and R. H. Huesman, "Reconstruction in PET cameras with irregular sampling and depth of interaction capability," *IEEE Trans. Nucl. Sci.*, vol. 45, pp. 1225–1230, June 1998.

[11] P. R. G. Virador, W. W. Moses, and R. H. Huesman *et al.*, "3-D reconstruction in PET cameras with irregular sampling and depth of interaction," *IEEE Trans. Nucl. Sci.*, vol. 48, pp. 1524–1529, Aug. 2001.

[12] R. H. Huesman, G. J. Klein, and W. W. Moses *et al.*, "List mode maximum likelihood reconstruction applied to positron emission mammography with irregular sampling," *IEEE Trans. Med. Imaging*, vol. 19, pp. 532–537, 2000.